Herman, F., Braun, J., Deal, E., Prasicek, G. (2018): The Response Time of Glacial Erosion. - *Journal of Geophysical Research*, *123*, pp. 801—817.

DOI: http://doi.org/10.1002/2017JF004586

Journal of Geophysical Research: Earth Surface

RESEARCH ARTICLE
10.1002/2017JF004586

Key Points:
- We derive analytically the response time of glacial erosion
- The analytical solution is tested with a numerical model
- An increase of glacial erosion during the Quaternary is physically plausible

Correspondence to:
F. Herman,
frederic.herman@unil.ch

Citation:
Herman, F., Braun, J., Deal, E., & Prasicek, G. (2018). The response time of glacial erosion. *Journal of Geophysical Research: Earth Surface*, *123*, 801–817. https://doi.org/10.1002/2017JF004586

Received 8 DEC 2017
Accepted 16 MAR 2018
Accepted article online 22 MAR 2018
Published online 26 APR 2018

The Response Time of Glacial Erosion

Frédéric Herman[1], Jean Braun[2,3], Eric Deal[2,4], and Günther Prasicek[1]

[1]Institute of Earth Surface Dynamics, University of Lausanne, Lausanne, Switzerland, [2]Helmholtz Centre Potsdam, GFZ German Research Center for Geosciences, Potsdam, Germany, [3]Institute of Earth and Environmental Science, University of Potsdam, Potsdam, Germany, [4]Department of Earth, Atmospheric and Planetary Sciences, Massachusetts Institute of Technology, Cambridge, MA, USA

Abstract There has been recent progress in the understanding of the evolution of Quaternary climate. Simultaneously, there have been improvements in the understanding of glacial erosion processes, with better parameter constraints. Despite this, there remains much debate about whether or not the observed cooling over the Quaternary has driven an increase in glacial erosion rates. Most studies agree that the erosional response to climate change must be transient; therefore, the time scale of the climatic change and the response time of glacial erosion must be accounted for. Here we analyze the equations governing glacial erosion in a steadily uplifting landscape with variable climatic forcing and derive expressions for two fundamental response time scales. The first time scale describes the response of the glacier and the second one the glacial erosion response. We find that glaciers have characteristic time scales of the order of 10 to 10,000 years, while the characteristic time scale for glacial erosion is of the order of a few tens of thousands to a few million years. We then use a numerical model to validate the approximations made to derive the analytical solutions. The solutions show that short period forcing is dampened by the glacier response time, and long period forcing (>1 Myr) may be dampened by erosional response of glaciers when the rock uplift rates are high. In most tectonic and climatic conditions, we expect to see the strongest response of glacial erosion to periodic climatic forcing corresponding to Plio-Pleistocene climatic cycles. Finally, we use the numerical model to predict the response of glacial systems to the observed climatic forcing of the Quaternary, including, but not limited to, the Milankovich periods and the long-term secular cooling trend. We conclude that an increase of glacial erosion in response to Quaternary cooling is physically plausible, and we show that the magnitude of the increase depends on rock uplift and ice accumulation rates.

1. Introduction

One of the best-documented transitions of Earth's climate history is the cooling that has occurred during the last 10 Myr. This cooling has led to the onset of Northern Hemisphere glaciations, which proceeded throughout the Pleistocene and continue today. While the exact timing of onset of glaciation in middle- to high-latitude mountain ranges remains uncertain, a high-resolution record of oxygen isotope measurements on foraminifera deposited on the ocean floor (Lisiecki & Raymo, 2005; Zachos et al., 2001) testifies that global climate has continuously fluctuated between times of relative warmth and coldness, with periods about 23, 41, and 100 kyr, as dictated by Milankovitch orbital forcings. Furthermore, thanks to the advent of new proxies for estimating how sea surface temperature varied through time, it is now thought that temperatures have dropped by 10 to 15°C during the last 10 Myr (Herbert et al., 2016). The magnitude of the temperature drop mainly depends on latitude and is more pronounced toward the poles than at the equator. Several studies argue that this climate transition may have caused a widespread increase of erosion based on an observed increased terrigenous sediment flux to ocean basins (Molnar & England, 1990), increased sedimentation rate in continental basins (Molnar, 2004; Zhang et al., 2001) and thermochronologically derived erosion rates in the last few million years (Herman & Champagnac, 2016; Herman et al., 2013; Shuster et al., 2005, 2011; Valla et al., 2012). An alternative perspective suggests that the widespread increase in erosion rates is an artifact, citing the Sadler effect (Ganti et al., 2016; Willenbring & von Blanckenburg, 2010; Willenbring & Jerolmack, 2016). The Sadler effect implies that the observed increase of erosion rates toward the present is caused by the intermittency of erosional processes (Finnegan et al., 2014; Ganti et al., 2016) as well as the incompleteness of the sedimentation record (Barrell, 1917; Sadler & Jerolmack, 2015, 2009; Tipper, 1983).

The debate over these two perspectives exists within the framework of the null hypothesis, which is the idea that over long time scales, landscapes are at, or close to, steady state and that erosion rates are determined solely by tectonic uplift rates (von Blanckenburg, 2005; Willenbring & von Blanckenburg, 2010; Willenbring & Jerolmack, 2016). Any increase in erosion rate due to a shift in climate is a transient response, which leads to the conclusion that over the long term, climate is a much less important driver of erosion than tectonics. The null hypothesis is not in question. It stems ultimately from the conservation of mass, and it will prevail as long as tectonic rates globally are roughly constant through time. However, the time scale over which the null hypothesis becomes accurate is less known. It will be determined by the longest period that a landscape can sustain a transient erosional response. If landscapes, particularly glacial landscapes, cannot or do not sustain transient conditions for as long as the secular cooling trend, then the observation of widespread increased erosion over the last 5 Myr must be related to the Sadler effect (assuming constant tectonic rate). On the other hand, if landscapes can sustain transient conditions for 1–10 Myr, then an erosional response to secular cooling is physically plausible, and such a response may then be recorded.

There is ample evidence that geomorphic processes such as fluvial and glacial erosion are transient across different time scales (Ganti et al., 2016; Koppes & Montgomery, 2009), but the characteristic time and maximum time over which geomorphic processes respond to climate change is not established for all erosional processes. This characteristic time must be established to estimate the time scale over which a landscape can sustain the transient conditions. Work using the stream power model for fluvial erosion implies maximum time scales up to a few million years, depending on uplift rate, erosional efficiency, spatial scale, and sustained transient conditions during the late Cenozoic (Braun et al., 2015; Whipple, 2001). Here our objective is to now estimate the response time for glacial erosion.

To estimate the glacial erosion response time, one needs constraints on the glacial erosion processes. Although there has been great progress in modeling glacial erosion processes (e.g., Braun et al., 1999; Egholm et al., 2009, 2011; Harbor et al., 1988; Kessler et al., 2008; MacGregor et al., 2000; Oerlemans, 1984; Pedersen et al., 2014; Sternai et al., 2013), the use of glacial erosion models has in part been hampered by a lack of observational constraints. It is thought that glaciers erode the underlying bedrock mainly through abrasion and plucking, which theories predict to be proportional to the ice sliding velocity raised to some power (Hallet, 1979, 1981, 1996; Iverson, 1990, 2012). Recently, two independent studies, one in the Antarctic Peninsula and the Patagonian Andes (Koppes et al., 2015) and the other on the Franz Josef Glacier (Herman et al., 2015), simultaneously collected erosion rate and ice velocity data to find that erosion rate depends nonlinearly on sliding velocity and that the exponent on velocity is about 2. Previous field studies had suggested a linear relationship between sliding velocity and erosion rate (Humphrey & Raymond, 1994; Tomkin & Braun, 2002) but relied on data collected from a surging glacier in Alaska combined with spatially averaged data from glaciers in the Alps and Norway. Interestingly, Koppes et al. (2015) and Herman et al. (2015) found very similar values for the proportionality constant, and the range of acceptable values reported in both studies includes the estimates of Humphrey and Raymond (1994). Altogether, these recent results provide new constraints on glacial erosion rules that can be implemented in landscape evolution models.

By taking advantage of the recent progress in deciphering Quaternary climate and understanding glacial erosion processes, as described above, we propose to estimate the response of glacial erosion to variable forcings imposed by late Cenozoic climate and tectonics. We start by deriving an analytical solution for two characteristic time scales for the ice response and erosion response of a glacier eroding an uplifting landscape. We then use a 1-D numerical model to estimate the response of glacial erosion to various forcings. The numerical model enables us to validate the analytical solution and include more feedbacks between topography, mass balance, and erosion. Finally, using existing constraints on the late Cenozoic cooling, we estimate how climate may have potentially modulated glacial erosion depending on precipitation (or ice accumulation) and rock uplift rates. It is worth stressing that we only concentrate on glacial erosion, even though it is clear that other processes, such as fluvial or hillslope erosion, have played a fundamental role for the global response of mountain erosion to late Cenozoic cooling.

2. Glacial Erosion Model

The evolution of mountain topography is governed by the competition between rock uplift and glacial erosion, which can be summarized by the following equation:

$$\frac{\partial z}{\partial t} = U - \dot{e} \tag{1}$$

Table 1
Variables Description and Values Used for the Analytical Solutions and the Numerical Model

Variable	Symbol	Value	Units
Glacial erosion response time	τ_e	10^4 to 10^7	year
Glacier response time	τ_i	10 to 10^4	year
Deformation flow parameter	f_d	4.2×10^{-5}	1/m^3 year
Sliding parameter	f_s	1.27	1/m year
Glen flow law exponent	n	3	—
Glacial erosion law constant	K_g	10^{-7} to 10^{-4}	m^{1-l}/year^{1-l}
Glacial erosion law exponent	l	1 to 2	—
Maximum accumulation rate	c	0.1 to 3	m/year
Mass balance rate gradient	β	0.005	1/year
Net mass balance	A	-	m/yr
Rock uplift rate	U	0.1 to 10	mm/year
Erosion rate	$\dot{e}$	—	mm/year
Bedrock elevation	z	—	m
Time	t	—	year
Ice thickness	H	—	m
Ice surface elevation	h	—	m
Slope	S	—	—
Equilibrium line altitude	E	1,000 to 2,000	m
Ice velocity	u	—	m/year
Ice sliding velocity	u_s	—	m/year
Ice deformation velocity	u_d	—	m/year
Glacier characteristic length	L	0 to 40	km

Note. A range of values is reported for variables that are varied. No value is provided for the variables that are model outcome.

where z is bedrock elevation, U is rock uplift rate, $\dot{e}$ is glacial erosion rate, and t is time. Glacial erosion rate is assumed to be proportional to the sliding velocity raised to some power (Hallet, 1979, 1981, 1996; Herman et al., 2015; Humphrey & Raymond, 1994; Iverson, 1990, 2012; Koppes et al., 2015):

$$\dot{e} = K_g |u_s|^l \tag{2}$$

where K_g is the glacial erosion rate constant, and l is an exponent. K_g is thought to vary between about 10^{-4} and 10^{-7} (m^{1-l}/year^{1-l}), depending on the choice of the exponent l between 1 and 2. To model erosion, one needs to compute the sliding velocity, which can be estimated from the ice thickness and ice surface slope. This can be achieved by solving the mass conservation equation:

$$\frac{\partial H}{\partial t} = A - \nabla \cdot \mathbf{q} \tag{3}$$

where H is the ice thickness, A is the net mass balance, and $\mathbf{q}$ is the ice flux. The net mass balance is given by

$$A = \min(\beta(h - E), c) \tag{4}$$

where β is the mass balance rate gradient, h is the ice surface elevation (i.e., $z + H$, where z is the bedrock elevation), c is a maximum ice accumulation rate, or cutoff, and E is the position the equilibrium line altitude (ELA).

The flux is the integral of the velocity over the ice thickness:

$$\mathbf{q} = H\bar{\mathbf{u}} \tag{5}$$

where $\bar{\mathbf{u}} = \mathbf{u_d} + \mathbf{u_s}$, and $\mathbf{u_d}$ is the deformation velocity. Assuming the shallow ice approximation (Hutter, 1983; Mahaffy, 1976), the vertically integrated velocity is given by

$$\bar{\mathbf{u}} = f_d H^{n+1} |\nabla h|^{n-1} \nabla h + f_s H^{n-1} |\nabla h|^{n-1} \nabla h \tag{6}$$

where the first term on the right-hand side is the deformation velocity and the second term is the sliding velocity. f_d and f_s are the flow parameters for deformation and sliding, respectively, and n is the Glen flow law exponent, which is often assumed equal to 3. Here the flow parameters are taken from Oerlemans (1997) who used values from Budd et al. (1979). In Table 1, we summarize the values of the main variables that are used in the following sections.

3. Characteristic Time Scales

Our objective is to derive analytical expressions for glacier and glacial erosion response times. This is done assuming a fixed accumulation rate, A, above the ELA. A is thus lower or equal to c. Combining equations (1), (2), and (6) and introducing the following dimensionless variables,

$$H' = H/H_0 \quad z' = z/z_0 \quad x' = x/L \quad t' = t/\tau_e \quad S' = S/S_0 \tag{7}$$

where x is for horizontal distance, S is for slope, L is the length of the glacier, and τ_e is the erosion response time scale we wish to derive. The subscript 0 is for characteristic variables. The characteristic topographic slope is defined as

$$S_0 = z_0/L \tag{8}$$

Using these variables and equation (1), we can write the following dimensionless equation:

$$\frac{z_0}{\tau_e}\frac{\partial z'}{\partial t'} = U - K_g f_s^l H_0^{(n-1)l}\left(\frac{z_0}{L}\right)^{nl}(H'^{n-1}S'^n)^l \tag{9}$$

and a natural value for the erosion response time, τ_e, is

$$\tau_e = \frac{L^{nl}}{K_g f_s^l H_0^{(n-1)l} z_0^{nl-1}} \tag{10}$$

or, after eliminating z_0

$$\tau_e = \frac{L}{K_g^{1/nl} f_s^{1/n} H_0^{1-1/n} U^{1-1/nl}} \tag{11}$$

which can be used to derive the characteristic topographic height, z_0:

$$z_0 = \frac{L U^{1/nl}}{K_g^{1/nl} f_s^{1/n} H_0^{1-1/n}} \tag{12}$$

or the characteristic topographic slope, $S_0 = z_0/L$:

$$S_0 = \frac{U^{1/nl}}{K_g^{1/nl} f_s^{1/n} H_0^{1-1/n}} \tag{13}$$

These three characteristic scales depend on H_0, which must be estimated. Assuming that the ice surface slope is mostly controlled by the bedrock slope, which is the case for high relief areas, and using our dimensionless variables, equation (3) becomes

$$\frac{H_0}{\tau_i}\frac{\partial H'}{\partial t'} = A + \frac{H_0^n z_0^n f_s}{L^{n+1}}\left(H'^n + \frac{H_0^2 f_d}{f_s}H'^{n+2}\right)S'^n \tag{14}$$

Taking the convention that $\tau_i = A/H_0$, the ice, or glacier, characteristic time scale, τ_i, can be derived:

$$\tau_i = \frac{L^{1+1/n}}{f_s^{1/n} A^{1-1/n} z_0} \tag{15}$$

and the characteristic ice thickness, H_0:

$$H_0 = \frac{L^{1+1/n} A^{1/n}}{f_s^{1/n} z_0}. \tag{16}$$

Combining equations (12) and (16) yields the following expression for z_0:

$$z_0 = \frac{L^{1/n} U^{1/l}}{K_g^{1/l} f_s^{1/n} A^{1-1/n}} \tag{17}$$

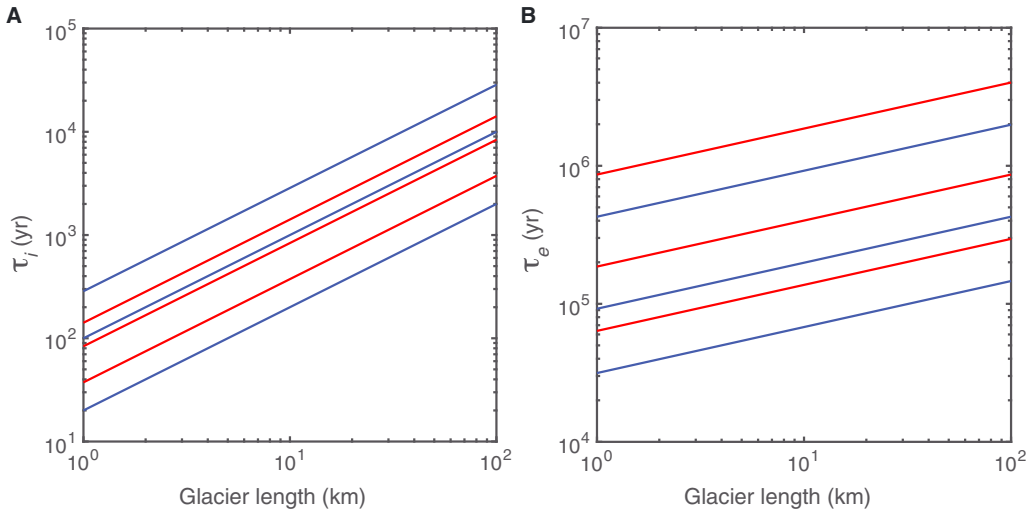

Figure 1. Characteristic time scales. The blue curves are for $l = 1$, and red curves are for $l = 2$. (a) Glacier response time. The three curves are for rock uplift rates, U, equal to 0.35, 1, and 5 mm/year, going from top to bottom. K_g is equal to 10^{-4} for $l = 1$ and $K_g = 7 \times 10^{-6}$ year/m for $l = 2$. (b) Glacial erosion response time. U is equal to 0.35 mm/year and A is equal to 0.1, 1, and 5 m/year from top to bottom. K_g is equal to 10^{-4} for $l = 1$ and $K_g = 7 \times 10^{-6}$ year/m for $l = 2$.

and H_0:

$$H_0 = LA\left(\frac{K_g}{U}\right)^{1/l} \tag{18}$$

From these expressions we can finally derive τ_i:

$$\tau_i = L\left(\frac{K_g}{U}\right)^{1/l} \tag{19}$$

and the glacial erosion response time, τ_e:

$$\tau_e = \frac{L^{1/n}}{K_g^{1/l} f_s^{1/n} A^{1-1/n} U^{1-1/l}} \tag{20}$$

and the characteristic surface topography slope, S_0:

$$S_0 = h_0/L = \frac{U^{1/l}}{K_g^{1/l} f_s^{1/n} A^{1-1/n} L^{1-1/n}} \tag{21}$$

When the erosion model is linear (i.e., $l = 1$), the glacier response time is directly proportional to L and inversely proportional to U:

$$\tau_i \propto \frac{L}{U} \tag{22}$$

Similar equations have been developed in other studies (e.g., Jóhannesson et al., 1989; Oerlemans, 2001, 2008, 2012; Roe & O'Neal, 2009; Roe et al., 2017), and all reach the conclusions that the glacier response time is proportional to its length divided by a characteristic velocity. Here we use rock uplift rate, as it has the dimensions of velocity and has a first-order effect on setting the characteristic slope, and thus ice thickness and ice sliding velocity. In addition, τ_e is controlled mostly by the accumulation rate and, to a lesser degree, by the length of the glacier:

$$\tau_e \propto \frac{L^{1/3}}{A^{2/3}} \tag{23}$$

Interestingly, the glacial erosion response time seems independent of the rock uplift rate. However, one should keep in mind that the length, L, is set by U. Higher uplift rate leads to steeper topography (equation (21)), and in the turn a longer glacier, and the response is not strictly independent of U, as discussed further below.

When the erosion model is quadratic (i.e., $l = 2$), the glacier response time scale dependence on uplift rate becomes

$$\tau_i \propto \frac{L}{U^{1/2}} \tag{24}$$

and the erosion response time becomes dependent on the inverse of square root of the uplift rate:

$$\tau_e \propto \frac{L^{1/3}}{A^{2/3}U^{1/2}} \tag{25}$$

In Figure 1, we compute the response times for realistic values of U, L, A, l, and K_g. Under a set of parameter values based on observations, the glacier response time varies between ten and a few thousand years, which is similar to other estimates (Oerlemans, 2012). In contrast, the glacial erosion characteristic time is much longer. It ranges from tens of thousands to a few million years. This result implies that while the glacier will respond to short-term variations (10–100 years), it will take much longer (i.e., 10 kyr to 10 Myr) for glacial erosion to reequilibrate with rock uplift rates in response to changes in climate forcings. This result indicates that the time scale for glacial erosion to reequilibrate is about the same order, or larger than Milankovitch cycles.

4. Steady State Topography and Time-Dependent Erosion Using a Numerical Model

We use a numerical solution to test the predicted time scales. A numerical solution is required because erosion and uplift modify topography and mass balance, which set the glacier length and in turn make the problem nonlinear. It also provides us with a means to test our analytical solution and relax the assumption that the accumulation rate is constant. We solve equations (2) to (6) in one dimension using the finite difference method. A linearly decreasing topography is assumed as initial condition. A fixed elevation on bedrock is used at the bottom of the model domain, and a no ice flux boundary condition is imposed at the top. For numerical stability a maximum hillslope threshold of 30° is imposed for the top bedrock of the model. Artificial linear diffusion is included where the ice thickness is less than 1 m and is kept as small as possible. Where there is no ice, erosion rate is set equal to rock uplift rate, and the topography does not change. Finally, we calculate how glacial erosion rates vary by monitoring the mean glacial erosion rate over the entire length of the glacier, since we are only investigating the response of glacial erosion to climate forcings, and do not explore the feedbacks with other geomorphic processes. In addition, the parameter values are informed by the latest observational constraints (Herman et al., 2015; Koppes et al., 2015).

Below we start by assessing a steady state situation. Then we analyze the behavior of the system in a situation where climate cools dramatically. Cooling is prescribed by lowering the ELA.

4.1. Steady State Longitudinal Profiles

In this section, we report a series of steady state solutions to illustrate how the topography varies as a function of rock uplift and maximum ice accumulation rates. The model is run for a fixed ELA until steady state between erosion and uplift is reached.

The first results illustrate the effect of varying uplift rate on steady state topography (Figure 2a). In case of low rock uplift rates, the model produces a concave profile, with the largest curvature about the ELA. More importantly, the glacier erodes the zone above the ELA substantially and in turn reduces the accumulation area. This result is consistent with previous modeling results (e.g., Braun et al., 1999; Egholm et al., 2009; MacGregor et al., 2000; Oerlemans, 1984; Pedersen et al., 2014; Sternai et al., 2013) and the idea that glacial erosion may limit the mean height of mountain ranges about the ELA (Egholm et al., 2009). In contrast, when we increase the rock uplift rate, the topographic profile becomes steeper and the glacier thinner. By raising the topographic gradient, glacial erosion increases and balances rock uplift rates.

Varying the maximum accumulation rates, c, has the opposite effect of varying the rock uplift rate (Figure 2b). Topography becomes steeper when the accumulation rate decreases. At low accumulation rate, which is equivalent to dry conditions, the ice flux and sliding velocities are low and the slope must increase to reach steady state.

An implication of these simple modeling results is that at high uplift rates and/or low accumulation rates the glacier must be steep and thin, and thus long, for erosion to balance uplift. Therefore, there exists a relationship between glacier length and rock uplift or maximum accumulation rates. In Figure 3a, we show how

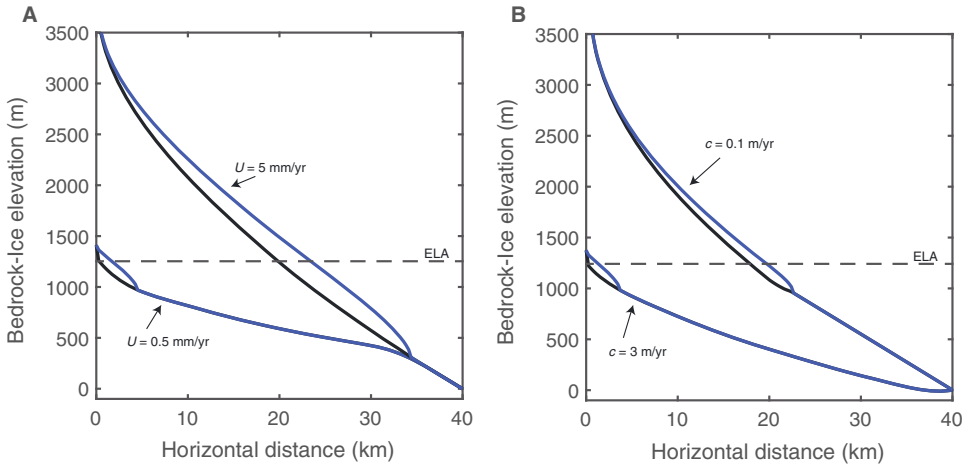

Figure 2. Steady state topography. (a) Topography and ice profiles for two different rock uplift rates of 0.5 and 5 mm/year, respectively. The maximum accumulation rate, *c*, is 1 m/year. (b) Topography and ice profiles for two different maximum accumulation rates of 0.1 and 3 m/year, respectively. The rock uplift rate is 1 mm/year. All models are run using $l = 2$, $K_g = 7 \times 10^{-6}$ year/m, and $\beta = 0.005$ 1/year. *E*, the position of the equilibrium line altitude, is 1,250 m.

the glacier varies with increasing uplift rate. It shows that the glacier as a function of uplift rate follows a logistic function. The glacier grows rapidly for uplift rates between 0 and 2 mm/year and reaches a maximum length for uplift rates higher than 4 mm/year. Given that for most mountainous areas the uplift rate is less than 4 mm/year, this effect is significant. In Figure 3b, we observe the inverse relationship with the maximum accumulation rates. For low accumulation rate, the glacier must be long to balance rock uplift rate. The glacier becomes shorter when accumulation rate increases.

The relationship we observe between *L*, the length of the glacier, and *U*, the uplift rate when the system has reached steady state, that is, such that $U = \dot{e} = K_g|u_s|^l$, can also be derived semianalytically and yields the following relationship between *L* and *U* (Appendix A):

$$L \propto U^{(n-1)/2nl} \tag{26}$$

that is in agreement with the results we obtain with the numerical model (Figure 3a).

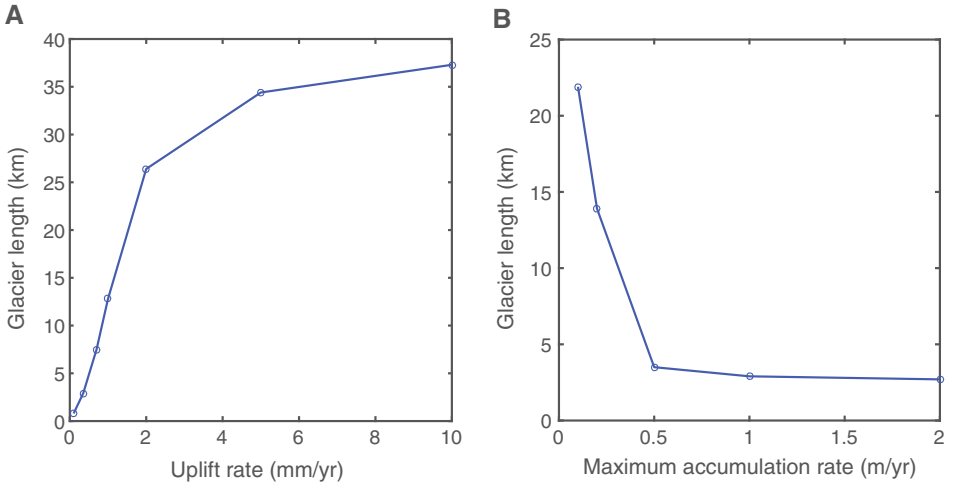

Figure 3. Relationship of glacier length versus uplift and glacier length versus accumulation at erosional steady state. A maximum accumulation rate of 1 m/year was used for (a) and a rock uplift rate of 0.35 mm/year was used for (b). All models are run using $l = 2$, $K_g = 7 \times 10^{-6}$ year/m, and $\beta = 0.005$ 1/year. *E*, the position of the equilibrium line altitude, is 1,250 m.

This relationship implies that the scaling we derived for the two time scales, τ_e and τ_i, becomes

$$\tau_e \propto \frac{U^{(2n^2(1-l)+n-1)/(2n^2l)}}{K_g^{1/l} f_s^{1/n} A^{1-1/n}} \tag{27}$$

and

$$\tau_i \propto \frac{K_g^{1/l}}{U^{(n+1)/(2nl)}} \tag{28}$$

or for $l = 1$ and $n = 3$:

$$\tau_e \propto \frac{U^{1/9}}{K_g f_s^{1/3} A^{2/3}} \propto A^{-2/3} \tag{29}$$

and

$$\tau_i \propto U^{-2/3} \tag{30}$$

and for $l = 2$ and $n = 3$:

$$\tau_e \propto \frac{U^{-4/9}}{K_g^{1/2} f_s^{1/3} A^{2/3}} \propto U^{-4/9} A^{-2/3} \tag{31}$$

and

$$\tau_i \propto U^{-1/3} \tag{32}$$

From these derivations, one can see that τ_e scales with climate in the linear erosion law and scales both with tectonics and climate for the quadratic erosion rule. It is worth stressing that we only derived a scaling relation. From this result is therefore not possible to calculate the exact response times. Instead, the scaling relation provides a means to estimate how the relation between the uplift rate and length affects the time response in a time-dependent model.

The relationship between uplift/accumulation rate and glacier length is important. It has been shown that the glacier sensitivity to change in the position of the ELA depends on its length (Oerlemans, 2001, 2012):

$$\frac{\mathrm{d}L}{\mathrm{d}E} = -\frac{2}{S_0} + \frac{2}{S_0}\frac{\partial H_0}{\partial L}\frac{\mathrm{d}L}{\mathrm{d}E} \tag{33}$$

Assuming that the second term on the right-hand side is negligible (Oerlemans, 2001, 2012), climate sensitivity is inversely proportional to the characteristic slope, S_0. Steep glaciers observed under high rock uplift rate and/or low maximum accumulation rates are thus less sensitive to changes in the position of the ELA. This has important implications when estimating the response time of a glacier with a time dependent solution, as we show below.

Finally, these modeling results also show that rock uplift rates and accumulation rates affect the ratio between accumulation and ablation areas. Obviously, one must keep in mind that such steady state conditions may not necessarily be observable today.

4.2. Transient Response to a Drop of ELA

To estimate the glacial erosion response time to a change in the position of the ELA, we first run the model until steady state, and then drop the position of the ELA. Assuming different uplift, U, and maximum accumulation rates, c, and erosion parameters, K_g and l, we can verify the analytical solution.

The results show that a drop of ELA leads to an increase of erosion rates in all cases. The magnitude of the increase is inversely proportional to the uplift rate (Figure 4a). At high uplift rates, the change of erosion rate is small. This is in part because the glacier is steep, and thus less sensitive to changes in the position of the ELA. Furthermore, the response time, that is, the time to come back to equilibrium, is inversely proportional to uplift rate. For the chosen model length (40 km) and other model parameters, the response time varies from more than 1.5 Myr down to less than 300 kyr with uplift rate increasing from 0.35 mm/year to 3 mm/year. These results are consistent with our analytical solution, which predicts characteristic times of hundreds of thousands to millions of years (Figure 1b) and τ_e to be inversely proportional to the square root of the uplift rate.

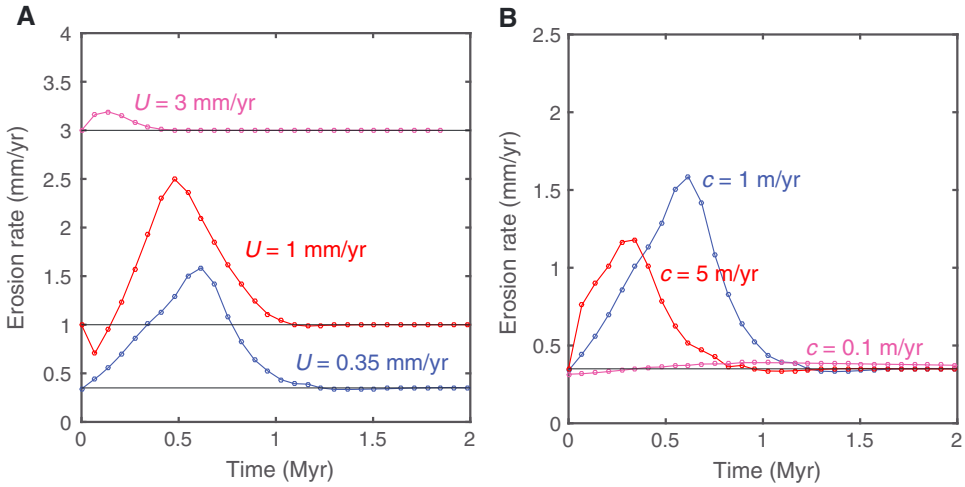

Figure 4. Response to a drop of equilibrium line altitude (ELA) for different uplift and maximum accumulation rates. (a) Erosion rate versus time for a drop of ELA from 1,250 to 1,000 m for different rock uplift rates. Blue, red, and magenta are for a rock uplift rate of 0.35, 1, and 3 mm/year, respectively. (b) Erosion rate versus time for a drop of ELA from 1,250 to 1,000 m for different maximum accumulation rates. Blue, red, and magenta are for an accumulation rate of 1, 5, and 0.1 m/year, respectively. All models are run using $l = 2$, $K_g = 7 \times 10^{-6}$ year/m, and $\beta = 0.005$ 1/year.

In the case of different maximum accumulation rates, we also observe that mean erosion rates increase when the ELA drops and that the amplitude of increase depends on the maximum accumulation rate (Figure 4b). The change in erosion rate is largest when the maximum accumulation rate is about 1 m/year and is very small when it is low (i.e., 0.1 m/year). The limited change in erosion rates under dry conditions can also be explained by the fact that the glacier is steep when the maximum accumulation rate is low (Figure 2b), which turn leads the glacier to be less sensitive to a drop of ELA. Furthermore, these numerical experiments show that the response time is inversely proportional to the maximum accumulation rate and ranges from about 1 Myr at high rates to several million years under dry conditions. Response times are much larger for changes in accumulation rate than for changes in uplift rate, which also consistent with the analytical solution that predicts the characteristic time to be inversely proportional to the accumulation rate raised to the power of 2/3.

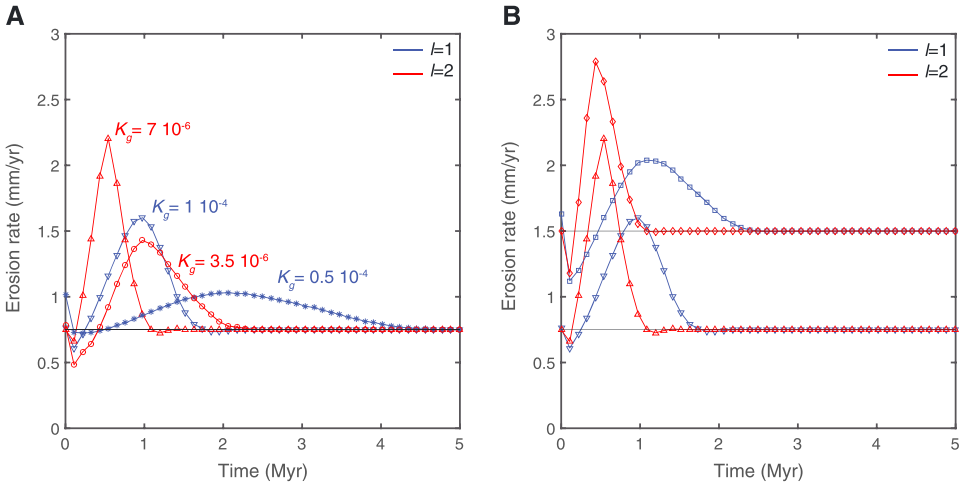

Figure 5. Response to a drop of equilibrium line altitude (ELA) for different K_g, l, and U. The blue lines are for l equal to 1 and red lines for l equal to 2. (a) Erosion rate versus time for a drop of ELA from 1,250 to 1,000 m, assuming a rock uplift rate of 0.75 mm/year, and a maximum accumulation rate of 1 m/year. (b) Erosion for a drop of ELA from 1,250 to 1,000 m, assuming different rock uplift rates. K_g is 1×10^{-4} when l is 1, and K_g is 7×10^{-6} when l is 2. All models are run using $\beta = 0.005$ 1/year.

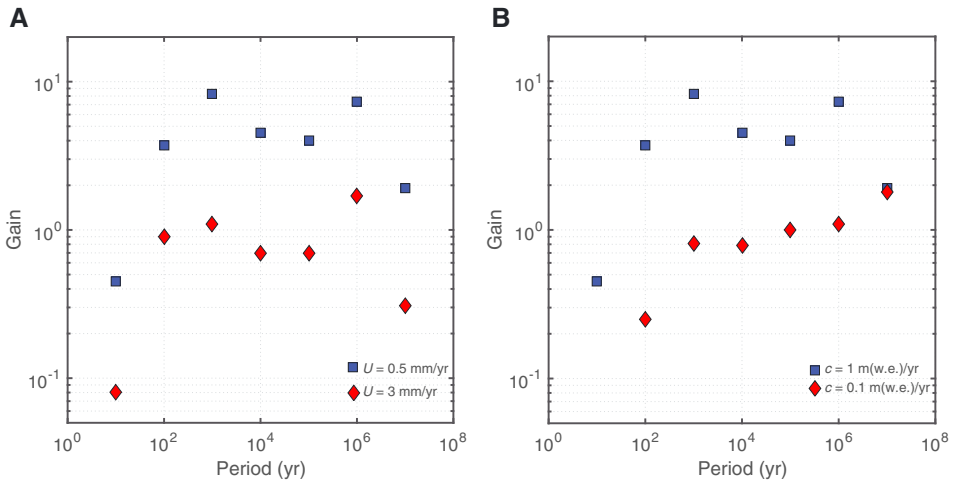

Figure 6. Gain as function of the forcing period. (a) Gain calculated at different forcing periods for two different uplift rates. Blue squares are for a rock uplift rate of 0.5 mm/year, and red diamonds are for a rock uplift rate of 3 mm/year. The maximum accumulation rate is 1 m/year. (b) Gain calculated at different forcing periods for two maximum accumulation rates. Blue squares are for a maximum accumulation rate of 1 m/year (same as [a]), and red diamonds are for a maximum accumulation of 0.1 m/year. The rock uplift rate is 0.5 mm/year. All models are run using $l = 2$, $K_g = 7 \times 10^{-6}$ year/m, and $\beta = 0.005$ 1/year.

Finally, we investigate the response to a change in ELA for different glacial erosion law constants, K_g, and erosion law exponents, l. The results show that the response time varies greatly with K_g (Figure 5a). Note that K_g is only constrained within an order of magnitude. Therefore, we must keep in mind that the response time can only be estimated within an order of magnitude. In any case, the numerical experiments show that τ_e increases when K_g decreases, regardless of l (Figure 5a). This result confirms the prediction of the analytical solution (equation (20)). More interestingly, we also observe that the response time is relatively insensitive to a change of uplift rate when l is 2 compared to 1 (Figure 5b). This may seem contradictory to equation (20). However, the length of the glacier, L, varies with the uplift rate (Figures 2 and 3 and equation (26)). As a result, the characteristic time increases with uplift rate when l is 1 and is less sensitive to a change in uplift rate when l is 2.

4.3. Response to a Periodic Forcing

A key part of our analysis is to assess how glacial erosion of uplifting mountain ranges responds to periodic forcings. In this section we then compute the gain, which corresponds to the ratio of output amplitude of oscillation (here the erosion times series predicted by the numerical model) to that of the input (the ELA periodic time series that is used as forcing), both normalized by their mean value. A gain of 1 means that there is no amplification or damping of the forcing. If the gain is less than one, the forcing is dampened, and a gain greater than 1 signifies that the perturbation is amplified by the system.

Here we vary the ELA as a periodic time series with an amplitude of 100 m for periods from 10 years to 10 Myr. The results are shown in Figure 6. Note that for long periods and low uplift rates, the glacier becomes very small at steady state, so we limit our analysis to examples of relatively high rock uplift rates (0.5–3 mm/year), which remains representative of long-term mountain erosion rates. We also vary the maximum accumulation rate, c, between 0.1 and 1 m/year. The same setup as in Figure 2 is used.

The results show that the gain is higher than 1 for forcings with periods higher than 100 years and starts to decrease for periods longer than about 10 Myr, assuming a rock uplift rate of 0.5 mm/year and a maximum accumulation rate of 1 m/year. The amplification effect is observed for forcing periods that are longer than the glacier response time, τ_i, and shorter than the glacial erosion response, τ_e. The gain decreases when rock uplift rate increases, or the maximum accumulation rate decreases. These results agree with the analytical solution that predicts the glacial erosion response time to be inversely proportional to rock uplift rates and mass balance and that the glacier becomes insensitive to ELA changes when the uplift rate is high or the maximum accumulation rate is low.

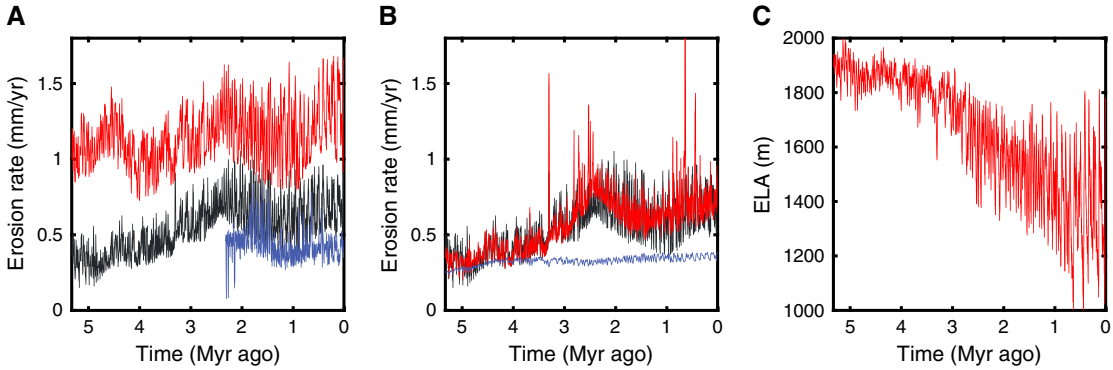

Figure 7. Glacial erosion response to late Cenozoic cooling. (a) Glacial erosion response for different rock uplift rates. The blue, black, and red curves are for uplift rates of 0.1, 0.35, and 1 mm/year, respectively. (Note that at low uplift rate, the glacier rapidly erodes the topography above the equilibrium line altitude [ELA], and glacial erosion only happens once the ELA is sufficiently low; (b) Glacial erosion response for different maximum accumulation rates. Blue, black, and red are for an accumulation rate 0.1, 1, and 5 m/year, respectively. (c) Prescribed ELA history. All models are run for $l = 2$, $K_g = 7 \times 10^{-6}$ year/m, and $\beta = 0.005$ 1/year.

5. Glacial Erosion Response to Late Cenozoic Cooling

In this final section, we estimate the glacial erosion response to the late Cenozoic cooling. First, we convert the δ^{18}O anomaly data (Lisiecki & Raymo, 2005) into an ELA anomaly. Given the sea surface temperature drop of about 5°C at midlatitudes (Herbert et al., 2016) during the last 5 Myr and assuming a moist temperature lapse rate of 5°C/km (Minder et al., 2010), we prescribe that the maximum drop in ELA was about 1 km during the last 5 Myr. The change in ELA is shown in Figure 7c. Note that the change may have been larger, and such an ELA drop may be seen conservative.

The results show that in all cases, glacial erosion rate increases in response to late Cenozoic cooling (Figure 7). The magnitude of the increase is inversely proportional to rock uplift rates. In the examples shown in Figure 7a, erosion rates are 4 times higher in the last 2 Myr compared to 5 Myr ago when the uplift rate is 0.1 mm/year, about twice higher when the rock uplift rate is 0.35 mm/year and 50% higher when the rock uplift rate is 1 mm/year. The decrease in the magnitude of change in erosion rates with increasing rock uplift rate is in part because the response time of glacial erosion is short and the glacier is steep, and thus less sensitive to changes in the position of the ELA.

The model responds very similarly for different maximum accumulation rates. Erosion rates become insensitive to the ELA drop under very dry conditions. This is also because the glacier is steep and insensitive to changes in the position of the ELA, even though the response time is very long. In contrast, erosion rates increase by about a factor of 2 when the maximum accumulation rate is higher than 1 m/year.

An alternative approach to examine the erosion response to some forcing is to compare the power density spectrum of forcing and erosion rate for different uplift and accumulation rates. Here we compute the power density spectrum using a discrete wavelet transform with the Morelet wavelet. The wavelet power spectrum is then calculated following the approach described in Torrence and Compo (1998) and implemented in MATLAB (Grinsted et al., 2004; Torrence & Compo, 1998).

We compare models with an ELA that is progressively lowering (blue curves in Figure 8) with one that has been detrended from the long-term cooling (red curves in Figure 8) and report three examples with varying rock uplift and maximum accumulation rates. The two forcings are shown in the inset of Figure 8a. The forcings' power spectra show that the power is maximized around 40 and 100 kyr and that the ELA time series that includes a long-term cooling contains additional power at a period of about 1.5 Myr.

In Figure 8b, we show the power spectra for the erosion rate history for the two forcings using a rock uplift rate of 0.5 mm/year and a maximum accumulation rate of 1 m/year. It shows that the erosion time series contains power around 40 and 100 kyr and that the forcing that includes a progressive cooling keeps power around 1.5 Myr, which is not the case for the detrended ELA history.

When the rock uplift rate is increased to 3 mm/year, the erosion rate time series retains power around the 40 and 100-kyr periods but contains no power for time scales greater than 1 Myr (Figure 8c). This is consistent

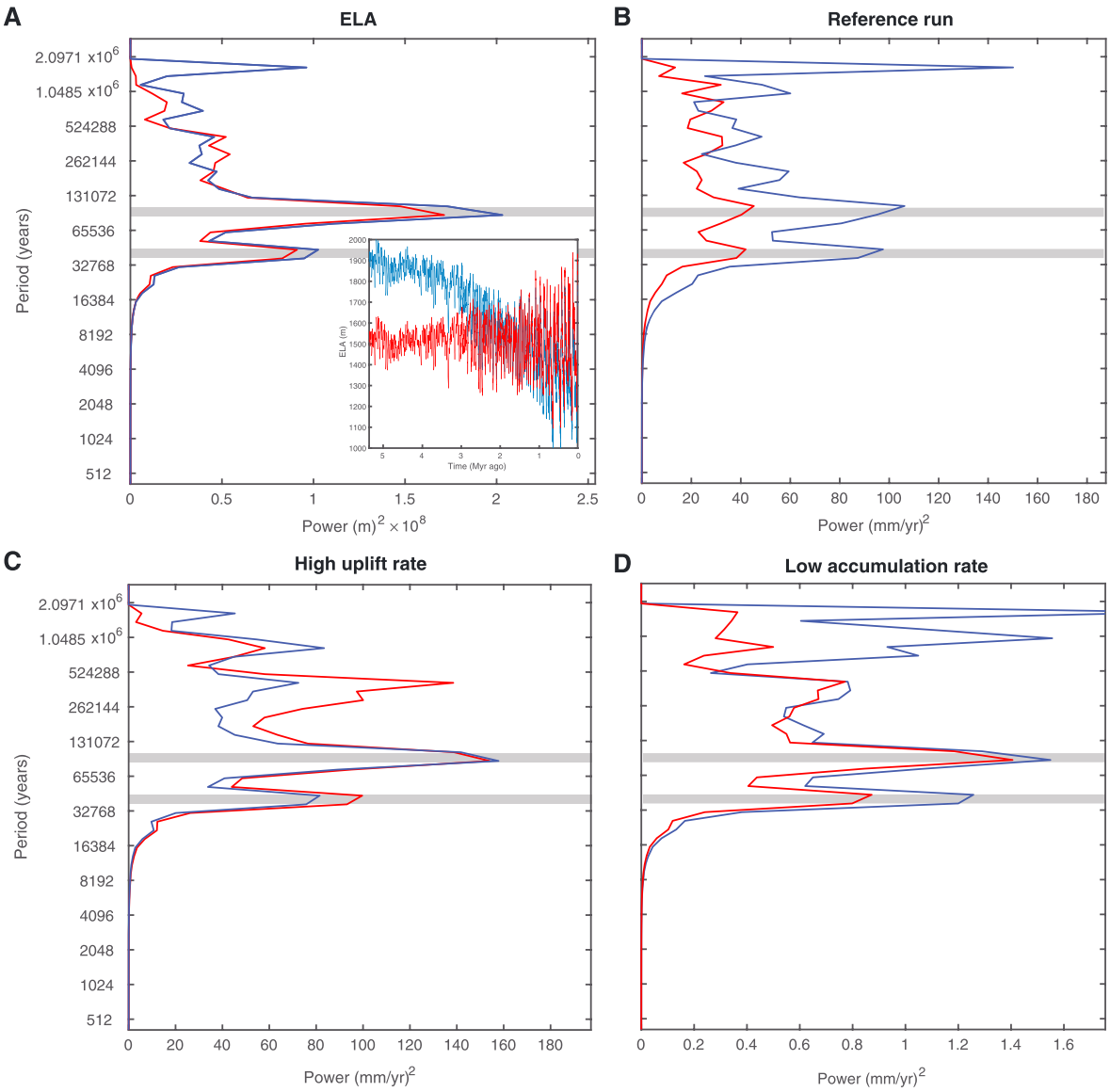

Figure 8. Power spectrum density. (a) Power spectrum of the forcing. The inset shows the equilibrium line altitude (ELA) time series used as forcings. The blue curve is for the same ELA time series as in Figure 7c, and the red curve is a detrended ELA time series (i.e., the long-term cooling trend has been removed). (b) Power spectra of the erosion rate history for a case where the rock uplift rate is 0.35 mm/year and max accumulation rate is 1 m/year. (c) is the same as (b) with the rock uplift rate that is increased to 3 mm/year. (d) Same as (b) with the maximum accumulation rate reduced to 0.1 m/year. All models are run using $l = 2$, $K_g = 7 \times 10^{-6}$ year/m, and $\beta = 0.005$ 1/year.

with our scaling of the time response of glacial erosion. Under high rock uplift conditions, the time response is shorter and the effect of climatic oscillations is dampened. In other words, the rock uplift rate is high enough for the topography to adjust to Myr climate variations, but it will still respond to Milankovitch cycles.

In the last case (Figure 8d), we decrease the maximum accumulation rate down to 0.1 m/year. It shows that power is retained in the power spectra, but the magnitude of the power is much smaller. Although the time response is large, the amplitude of changes remains small, as illustrated in Figure 4b.

Finally, this approach was not applied to the low rock uplift rate conditions. In that case, the topography is quickly eroded and the wavelet analysis makes less sense.

Altogether, these results confirm the idea that the response of glacial erosion might be strongest for climatic forcing corresponding to Plio-Pleistocene climatic cycles.

6. Discussion

Discussions about the impact of late Cenozoic cooling on erosion have been centered on the difficulty of finding direct observations for (e.g., Herman et al., 2013; Molnar, 2004; Zhang et al., 2001) or against an increase of erosion (e.g., Ganti et al., 2016; Willenbring & von Blanckenburg, 2010). The processes must be transient (Ganti et al., 2016; Herman et al., 2013; Koppes & Montgomery, 2009; Molnar, 2004; Willenbring & von Blanckenburg, 2010; Zhang et al., 2001), but estimates of characteristic time scales for glacial erosion are lacking. Here we take advantage of the most recent progress on the quantification of geomorphic processes, and on glacial erosion processes in this particular case, to calculate erosion rates for climate forcings varying differently with time. Our results show that the glacier characteristic time scale is between 10 and 10,000 years, which agrees with other studies (Oerlemans, 2012; Roe & O'Neal, 2009), and that the glacial erosion time scale ranges from ten thousand to ten million years, depending on rock uplift and ice accumulation rate.

The characteristic time for glacial erosion is comparable to Milankovitch cycles, but it also varies with rock uplift and maximum accumulation rates. We show that the glacial erosion response time varies as the inverse to the rock uplift rate and ice accumulation rate, but it also becomes insensitive to changes in the position of the ELA under higher rock uplift rates and dry conditions. This result has important implications, because one may expect to see the largest response to Quaternary glaciations in regions where the uplift rate is moderate (0.3 – 1 mm/year) and climate is wet. Indeed, recent studies that investigated the impact of glaciations on mountain erosion have suggested that the change in erosion may show a maximum at midlatitude (Champagnac et al., 2014; Haeuselmann et al., 2007; Shuster et al., 2005; Thomson et al., 2010; Valla et al., 2012), where ice accumulation rates were maximized during glacial periods. Furthermore, it has been observed that the highest change in erosion rates have been documented in tectonically moderate mountain ranges (Champagnac et al., 2014). Our results show that the increase may be as large as a factor of 4 in conditions of low rock uplift rates, up to a factor of 2 in more active places, and is less pronounced in very active mountain ranges (i.e., where the rock uplift rates are of the order of 5 mm/year).

Our results also highlight the important role of precipitation. Latitudinal patterns of glacial erosion are often attributed to temperature gradients. However, spatial variations of fluvial and glacial erosion at a global scale must be influenced by the patterns of precipitation associated with the westerly wind belts. Our results suggest that the response time and amplitude of changes is highly dependent on precipitation or ice accumulation rates. The response time of glacial erosion is long under dry conditions but the amplitude of erosion changes remains small. In other words, it seems unlikely to observe a large increase of erosion in dry places.

Our analysis suffers from several important limitations that could be tested with more sophisticated approaches. It neither includes other geomorphic processes, such as river incision or hillslope erosion, nor the feedbacks they may have with glacial erosion. It also ignores the effects of isostasy, which could increase the response time of glacial erosion to a time scale well beyond Milankovitch cycles (Ahnert, 1970; Braun et al., 2015). Similarly, the ice was treated as isothermal, even though the effects of cold-based conditions on glacial erosion and the evolution of topography are well documented (Garwood, 1910; Kleman & Stroeven, 1997; Sugden, 1968; Thomson et al., 2010; Tomkin & Braun, 2002). Finally, we show that the response time depends on the length scale and that glacier length depends on uplift and precipitation and have limited our numerical analysis to alpine type glaciers, that is, 10 – 40 km.

7. Conclusions

We have derived two expressions for two characteristic times for a glacier and its associated erosion in an uplifting mountain range, which we validated using a numerical model. The glacier response time scale, τ_i, is given by

$$\tau_i = L\left(\frac{K_g}{U}\right)^{1/l} \tag{34}$$

and the glacial erosion response time scale, τ_e, by

$$\tau_e = \frac{L^{1/n}}{K_g^{1/l} f_s^{1/n} A^{1-1/n} U^{1-1/l}} \tag{35}$$

τ_i is much shorter (10 years to 10 kyr) than τ_e (10 kyr to 10 Myr). The exact response times depend on the erosion parameters, K_g and l, and the rock uplift and accumulation rates.

These derived time scales, combined results from numerical simulation, lead us to conclude that short period forcing is dampened by the glacier response time and long period forcing (>1 Myr) may be dampened by the erosion response of glaciers when the rock uplift rates are high.

Our analysis shows that an increase of glacial erosion in response to Quaternary cooling is physically plausible. The magnitude of erosion increase due to late Cenozoic cooling is expected to vary locally depending on the tectonic and climate conditions. In particular, the response of glacial systems to the observed climatic forcing of the Quaternary, including the Milankovich periods and the long-term secular cooling trend, suggests the strongest response of glacial erosion to periodic climatic forcing corresponding to Plio-Pleistocene climatic cycles, but the magnitude of the increase depends highly on rock uplift and ice accumulation rates. The increase is expected to be highest in regions that are relatively wet and of moderate uplift rates (i.e., 0.3–1 mm/year).

Appendix A: Semianalytical Scaling Relationship Between Glacier Length and Uplift Rate

From equation (3), one can write that

$$q = -\int_0^x A(x)\,\mathrm{d}x \tag{A1}$$

and from equation (4), limited to the case where the maximum accumulation rate or cutoff, c, is never reached:

$$q = -\int_0^x \beta\ (z(x) + H(x) - E(x))\ \mathrm{d}x \tag{A2}$$

Assuming that the sliding velocity is much greater than the deformation velocity, which is only strictly valid for steep and wet glaciers, one can also write:

$$q = Hu_s = -\int_0^x \beta\ (z(x) + H(x) - E(x))\ \mathrm{d}x \tag{A3}$$

Differentiating this with respect to x leads to

$$\frac{\partial H}{\partial x} = -\frac{\beta}{u_s}(z + H - E) \tag{A4}$$

and, after further differentiation:

$$\frac{\partial^2 H}{\partial x^2} = -\frac{\beta}{u_s}\frac{\partial (z + H)}{\partial x} \tag{A5}$$

From the steady state assumption, one can write as follows:

$$u_s = f_s\left(\frac{\partial(z + H)}{\partial x}\right)^n H^{n-1} \tag{A6}$$

or, using the previous relationship:

$$u_s = f_s\left(\frac{u_s}{\beta}\right)^n \left(\frac{\partial^2 H}{\partial x^2}\right)^n H^{n-1} \tag{A7}$$

and the following relationship is obtained:

$$\left(\frac{\partial^2 H}{\partial x^2}\right)^n H^{n-1} = -\frac{\beta^n}{u_s^{n-1} f_s} = -C \tag{A8}$$

which shows that, at topographic steady state, at every point along a glacier, the product of the curvature of the ice thickness (to the power n) by the ice thickness (to the power $n - 1$) is a constant which we will call C:

$$C = \frac{\beta^n}{u_s^{(n-1)} f_s} = \frac{\beta^n}{(U/K_g)^{(n-1)/l} f_s} \tag{A9}$$

Assuming that in the vicinity of any point x along the glacier, the ice thickness can be approximated by a second-order Taylor expansion:

$$H(x-\epsilon) = H(x) - \epsilon\frac{\partial H}{\partial x}(x) + \epsilon^2\frac{\partial^2 H}{\partial x^2}(x) + O(\epsilon^3) \tag{A10}$$

We can derive a set of evolution equations from x to $x-\epsilon$ for the first- and second-order derivatives of the ice thickness:

$$\frac{\partial H}{\partial x}(x-\epsilon) = \frac{\partial H}{\partial x}(x) - \epsilon\frac{\partial^2 H}{\partial x^2}(x) + O(\epsilon^2) \tag{A11}$$

and

$$\frac{\partial^2 H}{\partial x^2}(x-\epsilon) = -C^{1/n}H^{-(n-1)/n}(x-\epsilon) \tag{A12}$$

and the bedrock height:

$$z(x-\epsilon) = -\frac{\partial H}{\partial x}(x-\epsilon)\frac{u_s}{\beta} + (E - H(x-\epsilon)) \tag{A13}$$

We can use these evolution equations to derive the thickness of the glacier $H(x)$ from the ELA down to the base of the glacier. At the ELA, that is, at $x = x_e$, we assume that the ice thickness is known $H(x) = H_e$. We also assume that the ice thickness does not change as the accumulation rate is nil. One can therefore write

$$H(x_e) = H_e; \quad \frac{\partial H}{\partial x}(x_e) = 0; \quad \frac{\partial^2 H}{\partial x^2} = C^{1/n}H_e^{-(n-1)/n} \tag{A14}$$

and

$$z(x_e) = E - H_e \tag{A15}$$

We call L_e the distance from x_e where the ice thickness goes to zero:

$$H(x_e - L_e) = 0 \tag{A16}$$

and make the assumption that this length is approximately equal to half the glacier length:

$$L = 2L_e \tag{A17}$$

After running a large number of computations varying all parameters, that is, U, K_g, β, H_e, we found that the length of the glacier scales as:

$$L \propto U^{(n-1)/2nl} \tag{A18}$$

regardless of the value of the other parameters.

Acknowledgments
Ann Rowan, Arjen Stroeven, and an anonymous reviewer are warmly thanked for their reviews. The codes are available through the Swiss Geocomputing Center at the University of Lausanne.

References

Ahnert, F. (1970). Functional relationships between denudation, relief, and uplift in large, mid-latitude drainage basins. *American Journal of Science*, *268*(3), 243–263.

Barrell, J. (1917). Rhythms and the measurements of geologic time. *Geological Society of America Bulletin*, *28*(1), 745–904.

Braun, J., Voisin, C., Gourlan, A., & Chauvel, C. (2015). Erosional response of an actively uplifting mountain belt to cyclic rainfall variations. *Earth Surface Dynamics*, *3*(1), 1–14.

Braun, J., Zwartz, D., & Tomkin, J. H. (1999). A new surface-processes model combining glacial and fluvial erosion. *Annals of Glaciology*, *28*(1), 282–290.

Budd, W., Keage, P., & Blundy, N. (1979). Empirical studies of ice sliding. *Journal of Glaciology*, *23*(89), 157–170.

Champagnac, J.-D., Valla, P. G., & Herman, F. (2014). Late-cenozoic relief evolution under evolving climate: A review. *Tectonophysics*, *614*, 44–65.

Egholm, D., Nielsen, S., Pedersen, V. K., & Lesemann, J.-E. (2009). Glacial effects limiting mountain height. *Nature*, *460*(7257), 884–887.

Egholm, D. L., Knudsen, M. F., Clark, C. D., & Lesemann, J. E. (2011). Modeling the flow of glaciers in steep terrains: The integrated second-order shallow ice approximation (iSOSIA). *Journal of Geophysical Research*, *116*, F02012. https://doi.org/10.1029/2010JF001900

Finnegan, N. J., Schumer, R., & Finnegan, S. (2014). A signature of transience in bedrock river incision rates over timescales of 10^4–10^7 years. *Nature*, *505*(7483), 391–394.

Ganti, V., von Hagke, C., Scherler, D., Lamb, M. P., Fischer, W. W., & Avouac, J.-P. (2016). Time scale bias in erosion rates of glaciated landscapes. *Science Advances*, *2*(10), e1600204.

Garwood, E. J. (1910). Features of alpine scenery due to glacial protection. *The Geographical Journal*, *36*(3), 310–336.

Grinsted, A., Moore, J. C., & Jevrejeva, S. (2004). Application of the cross wavelet transform and wavelet coherence to geophysical time series. *Nonlinear Processes in Geophysics*, *11*(5/6), 561–566.

Haeuselmann, P., Granger, D. E., Jeannin, P.-Y., & Lauritzen, S.-E. (2007). Abrupt glacial valley incision at 0.8 Ma dated from cave deposits in Switzerland. *Geology*, *35*(2), 143–146.
Hallet, B. (1979). A theoretical model of glacial abrasion. *Journal of Glaciology*, *23*(89), 39–50.
Hallet, B. (1981). Glacial abrasion and sliding: Their dependence on the debris concentration in basal ice. *Annals of Glaciology*, *2*(1), 23–28.
Hallet, B. (1996). Glacial quarrying: A simple theoretical model. *Annals of Glaciology*, *22*(1), 1–8.
Harbor, J. M., Hallet, B., & Raymond, C. F. (1988). A numerical model of landform development by glacial erosion. *Nature*, *333*(6171), 347–349.
Herbert, T. D., Lawrence, K. T., Tzanova, A., Peterson, L. C., Caballero-Gill, R., & Kelly, C. S. (2016). Late Miocene global cooling and the rise of modern ecosystems. *Nature Geoscience*, *9*, 843–847.
Herman, F., Beyssac, O., Brughelli, M., Lane, S. N., Leprince, S., Adatte, T., et al. (2015). Erosion by an alpine glacier. *Science*, *350*(6257), 193–195.
Herman, F., & Champagnac, J.-D. (2016). Plio-Pleistocene increase of erosion rates in mountain belts in response to climate change. *Terra Nova*, *28*(1), 2–10.
Herman, F., Seward, D., Valla, P. G., Carter, A., Kohn, B., Willett, S. D., & Ehlers, T. A. (2013). Worldwide acceleration of mountain erosion under a cooling climate. *Nature*, *504*(7480), 423–426.
Humphrey, N. F., & Raymond, C. (1994). Hydrology, erosion and sediment production in a surging glacier: Variegated Glacier, Alaska, 1982–83. *Journal of Glaciology*, *40*(136), 539–552.
Hutter, K. (1983). *Theoretical glaciology: Material science of ice and the mechanics of glaciers and ice sheets* (Vol. 1). Netherlands: Springer.
Iverson, N. R. (1990). Laboratory simulations of glacial abrasion: Comparison with theory. *Journal of Glaciology*, *36*(124), 304–314.
Iverson, N. R. (2012). A theory of glacial quarrying for landscape evolution models. *Geology*, *40*(8), 679–682.
Jóhannesson, T., Raymond, C., & Waddington, E. (1989). Time-scale for adjustment of glaciers to changes in mass balance. *Journal of Glaciology*, *35*(121), 355–369.
Kessler, M. A., Anderson, R. S., & Briner, J. P. (2008). Fjord insertion into continental margins driven by topographic steering of ice. *Nature Geoscience*, *1*(6), 365–369.
Kleman, J., & Stroeven, A. P. (1997). Preglacial surface remnants and Quaternary glacial regimes in northwestern Sweden. *Geomorphology*, *19*(1–2), 35–54.
Koppes, M., Hallet, B., Rignot, E., Mouginot, J., Wellner, J. S., & Boldt, K. (2015). Observed latitudinal variations in erosion as a function of glacier dynamics. *Nature*, *526*(7571), 100–103.
Koppes, M. N., & Montgomery, D. R. (2009). The relative efficacy of fluvial and glacial erosion over modern to orogenic timescales. *Nature Geoscience*, *2*(9), 644–647.
Lisiecki, L. E., & Raymo, M. E. (2005). A pliocene-pleistocene stack of 57 globally distributed benthic δ^{18}O records. *Paleoceanography*, *20*, PA1003. https://doi.org/10.1029/2004PA001071
MacGregor, K. R., Anderson, R., Anderson, S., & Waddington, E. (2000). Numerical simulations of glacial-valley longitudinal profile evolution. *Geology*, *28*(11), 1031–1034.
Mahaffy, M. (1976). A three-dimensional numerical model of ice sheets: Tests on the Barnes Ice Cap, Northwest Territories. *Journal of Geophysical Research*, *81*(6), 1059–1066.
Minder, J. R., Mote, P. W., & Lundquist, J. D. (2010). Surface temperature lapse rates over complex terrain: Lessons from the cascade mountains. *Journal of Geophysical Research*, *115*, D14122. https://doi.org/10.1029/2009JD013493
Molnar, P. (2004). Late Cenozoic increase in accumulation rates of terrestrial sediment: How might climate change have affected erosion rates? *Annual Review of Earth and Planetary Sciences*, *32*, 67–89.
Molnar, P., & England, P. (1990). Late cenozoic uplift of mountain ranges and global climate change: Chicken or egg? *Nature*, *346*(6279), 29–34.
Oerlemans, J. (1984). Numerical experiments on glacial erosion. *Zeitschrift für Gletscherkunde und Glazialgeologie*, *20*, 107–126.
Oerlemans, J. (1997). Climate sensitivity of Franz Josef Glacier, New Zealand, as revealed by numerical modeling. *Arctic and Alpine Research*, *29*, 233–239.
Oerlemans, J. (2001). *Glaciers and climate change*. Netherlands: CRC Press.
Oerlemans, J. (2008). *Minimal Glacier Models*. Igitur: Utrecht Publishing & Archiving Services.
Oerlemans, J. (2012). Linear modelling of glacier length fluctuations. *Geografiska Annaler: Series A, Physical Geography*, *94*(2), 183–194.
Pedersen, V. K., Huismans, R. S., Herman, F., & Egholm, D. L. (2014). Controls of initial topography on temporal and spatial patterns of glacial erosion. *Geomorphology*, *223*, 96–116.
Roe, G. H., Baker, M. B., & Herla, F. (2017). Centennial glacier retreat as categorical evidence of regional climate change. *Nature Geoscience*, *10*(2), 95–99.
Roe, G. H., & O'Neal, M. A. (2009). The response of glaciers to intrinsic climate variability: Observations and models of late-Holocene variations in the Pacific Northwest. *Journal of Glaciology*, *55*(193), 839–854.
Sadler, P. M., & Jerolmack, D. J. (2015). Scaling laws for aggradation, denudation and progradation rates: The case for time-scale invariance at sediment sources and sinks. *Geological Society, London, Special Publications*, *404*(1), 69–88.
Schumer, R., & Jerolmack, D. J. (2009). Real and apparent changes in sediment deposition rates through time. *Journal of Geophysical Research*, *114*, F00A06. https://doi.org/10.1029/2009JF001266
Shuster, D. L., Cuffey, K. M., Sanders, J. W., & Balco, G. (2011). Thermochronometry reveals headward propagation of erosion in an alpine landscape. *Science*, *332*(6025), 84–88.
Shuster, D. L., Ehlers, T. A., Rusmoren, M. E., & Farley, K. A. (2005). Rapid glacial erosion at 1.8 Ma revealed by ^{4}He/^{3}He thermochronometry. *Science*, *310*(5754), 1668–1670.
Sternai, P., Herman, F., Valla, P. G., & Champagnac, J.-D. (2013). Spatial and temporal variations of glacial erosion in the Rhône valley (Swiss Alps): Insights from numerical modeling. *Earth and Planetary Science Letters*, *368*, 119–131.
Sugden, D. (1968). The selectivity of glacial erosion in the Cairngorm Mountains, Scotland. *Transactions of the Institute of British Geographers*, *45*, 79–92.
Thomson, S. N., Brandon, M. T., Tomkin, J. H., Reiners, P. W., Vásquez, C., & Wilson, N. J. (2010). Glaciation as a destructive and constructive control on mountain building. *Nature*, *467*(7313), 313–317.
Tipper, J. C. (1983). Rates of sedimentation, and stratigraphical completeness. *Nature*, *302*(5910), 696–698.
Tomkin, J. H., & Braun, J. (2002). The influence of alpine glaciation on the relief of tectonically active mountain belts. *American Journal of Science*, *302*(3), 169–190.
Torrence, C., & Compo, G. P. (1998). A practical guide to wavelet analysis. *Bulletin of the American Meteorological Society*, *79*(1), 61–78.

Valla, P. G., van der Beek, P. A., Shuster, D. L., Braun, J., Herman, F., Tassan-Got, L., & Gautheron, C. (2012). Late Neogene exhumation and relief development of the Aar and Aiguilles Rouges massifs (Swiss Alps) from low-temperature thermochronology modeling and $^{4}He/^{3}He$ thermochronometry. *Journal of Geophysical Research*, *117*, F01004. https://doi.org/10.1029/2011JF002043

von Blanckenburg, F. (2005). The control mechanisms of erosion and weathering at basin scale from cosmogenic nuclides in river sediment. *Earth and Planetary Science Letters*, *237*(3), 462–479.

Whipple, K. X. (2001). Fluvial landscape response time: How plausible is steady-state denudation? *American Journal of Science*, *301*(4–5), 313–325.

Willenbring, J. K., & Jerolmack, D. J. (2016). The null hypothesis: Globally steady rates of erosion, weathering fluxes and shelf sediment accumulation during Late Cenozoic mountain uplift and glaciation. *Terra Nova*, *28*(1), 11–18.

Willenbring, J. K., & von Blanckenburg, F. (2010). Long-term stability of global erosion rates and weathering during late-Cenozoic cooling. *Nature*, *465*(7295), 211–214.

Zachos, J., Pagani, M., Sloan, L., Thomas, E., & Billups, K. (2001). Trends, rhythms, and aberrations in global climate 65 Ma to present. *Science*, *292*(5517), 686–693.

Zhang, P., Molnar, P., & Downs, W. R. (2001). Increased sedimentation rates and grain sizes 2–4 Myr ago due to the influence of climate change on erosion rates. *Nature*, *410*(6831), 891–897.